Int. J. Heat Mass Transfer. Vol. 30, No. 4, pp. 673–681, 1987
Printed in Great Britain

0017-9310/87 $3.00 + 0.00

Pressure drop during laminar oblique flow through in-line tube assemblies

K. A. ANTONOPOULOS

National Technical University of Athens, Mechanical Engineering Department, Thermal Section, 42 Patission Street, Athens 106 82, Greece

(*Received* 14 *October* 1985)

Abstract—The pressure drop values occurring during laminar, oblique, fully-developed flow through in-line tube assemblies of pitch-to-diameter ratios from 1.25 to 2.00 are calculated in detail. The inclination angle Θ of the mean velocity vector to the tube axes is varied in the range $0° \leqslant \Theta \leqslant 90°$. New information is provided on the influence of inclination angle on pressure drop. The method of calculation is based on a finite-difference solution of the momentum and continuity equations expressed in curvilinear–orthogonal coordinates. The method is validated by comparing the results with existing theoretical and experimental data in the limiting cases of purely axial ($\Theta = 0°$) and purely transverse ($\Theta = 90°$) flow, since such data are not available for $0° < \Theta < 90°$.

1. INTRODUCTION

ASSEMBLIES of parallel tubes, such as those illustrated in Fig. 1(a), feature in many types of industrial equipment. Fluids may flow both within and around the tubes, but it is the latter problem which is of interest here. Depending on the manner in which the fluid is introduced and the presence or not of baffles or other obstructions within the assembly, the flow may range in complexity from a simple fully-developed two-dimensional structure with streamlines aligned with the tube axes, to a three-dimensional flow with recirculation in all directions.

The case of primary interest here is the steady, laminar, uniformly oblique, fully-developed flow, i.e. the mean velocity vector is assumed to make an arbitrary but uniform angle Θ with the axes of the tubes (Fig. 1(a)). In the limiting case of inclination angle $\Theta = 0°$ the situation is referred to as purely 'axial' or 'parallel' fully-developed flow encountered, for example, in a nuclear reactor fuel assembly with the coolant flowing axially in the spaces between the fuel rods. For $\Theta = 90°$ the flow is purely 'transverse' or 'cross-flow' as, for example, in those steam boilers, condensers, evaporators and heat exchangers where the fluid is directed normal to the tube axes.

The pressure drop values occurring during the flow case referred to above are of great practical interest. The main object of the study is to calculate these

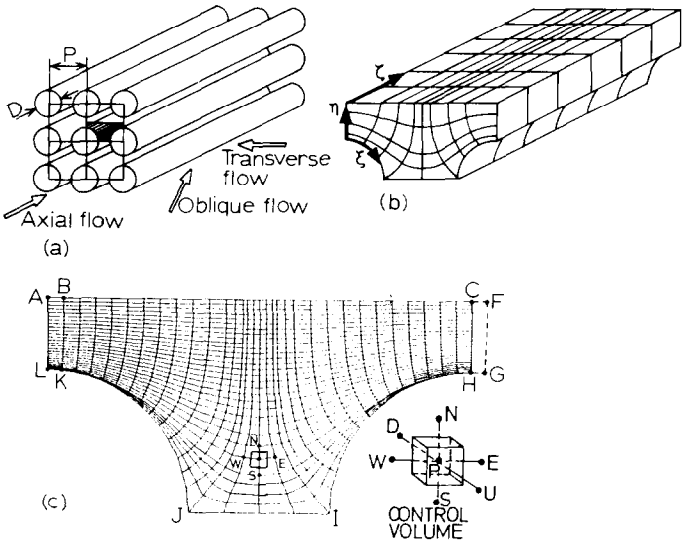

FIG. 1. Flow through in-line tube assemblies: (a) axial, transverse and oblique flow; (b) solution domain with computational grid and coordinate system; (c) typical computational grid in cross-sectional view and control volume.

NOMENCLATURE

a_n	coefficient in finite-difference equations
c_p	pressure drop coefficient in the direction of an oblique flow, $\Delta p/(0.5\rho\bar{V}^2)$
c_{pa}	axial pressure drop coefficient, $\bar{\tau}_\zeta/(0.5\rho\bar{w}^2)$
c_{pt}	transverse pressure drop coefficient, $\Delta p_v/(0.5\rho\bar{u}^2)$
D	tube diameter
h_ξ, h_η, h_ζ	metric coefficients associated with the coordinates $\xi, \eta\, \zeta$, respectively
P	distance between axes of adjacent tubes of the same row (pitch)
p	local pressure
Δp	pressure drop per row of tubes in the direction of an oblique flow
Δp_t	pressure drop per row of tubes in the transverse direction
Re	Reynolds number of an oblique flow, $(\rho\bar{V}D)/\mu$
Re_a	axial Reynolds number, $(\rho\bar{w}D)/\mu$
Re_t	transverse Reynolds number, $(\rho\bar{u}D)/\mu$
S_Φ	source term in the transport equations
$\bar{V}$	mean velocity of an oblique flow
u, v, w	velocity components in the ξ-, η-, and ζ-directions, respectively
$\bar{u}$	mean transverse velocity through the minimum gap
$\bar{w}$	mean axial velocity.

Greek symbols

ζ	rectilinear coordinate in the axial direction
ξ, η	curvilinear–orthogonal coordinates on the cross-sectional plane
Θ	angle of inclination of the bulk velocity to the tube axes, $\arctan(\bar{u}/\bar{w})$
μ	molecular viscosity
ρ	fluid density
τ_ξ, τ_ζ	wall shear stress in the ξ- and ζ-directions, respectively
$\bar{\tau}_\zeta$	average value of τ_ζ around the periphery of a tube
Φ	general dependent variable which may stand for u, v, w
φ	angular position of a point on the tube surface measured from the rear of the tube.

values in terms of the geometrical characteristics of the assembly, the inclination angle Θ and the Reynolds number of the flow. Other quantities as, for example, velocity and shear stress distributions are also calculated. The method of approach is numerical and based on a finite-difference solution of the momentum and continuity differential equations expressed in curvilinear–orthogonal coordinates. These allow the irregularly-shaped solution domain (Fig. 1(b)) to be mapped by a computational mesh which conforms to its shape. The method of solution is general and applicable to any tube bank geometry, as well as to more complex flow situations. However, attention here is confined to in-line square arrangements of pitch-to-diameter ratio P/D from 1.25 to 2.00. Reynolds numbers up to 500 are considered and the inclination angle Θ is taken to vary in the range $0° \leqslant \Theta \leqslant 90°$. The limiting cases of $\Theta = 0°$ and $90°$ are examined mainly for making comparisons of the results with existing theoretical and experimental data in order to assess the accuracy of the method, since such data are hardly available for $0° < \Theta < 90°$.

Although the fully-developed oblique flow in tube assemblies is of great practical interest, it has received very little attention, as implied above. Almost without exception, the studies thus far have been confined to the limiting cases of purely axial and purely transverse flow. The studies of Sparrow and Loeffler [1] (laminar, analytical), Meyder [2] (laminar, numerical), Rehme [3] (turbulent, experimental) and Carajelescov and Todreas [4] (turbulent, experimental and numerical) are typical of the first case while those of Bergelin *et al.* [5] (laminar, experimental), Zhukauskas [6] (turbulent, collection of data), Le Feuvre [7] and Massey [8] (laminar and turbulent, numerical) of the second. A review of pressure drop correlations is available in Kays and London [9] and ESDU [10]. A full survey of experimental and theoretical work on laminar and turbulent flow in tube assemblies may be found in ref. [11].

2. COORDINATE SYSTEM, GOVERNING EQUATIONS AND BOUNDARY CONDITIONS

The solution domain (unit of symmetry of flow) is a part of the channel formed by adjacent parallel tubes of the assembly as illustrated in Figs. 1(a) and (b). In order to map this domain by a coordinate frame so that all boundaries may be coordinate planes, the mixed coordinate system ξ–η–ζ, illustrated in Fig. 1(b), is employed: coordinates ξ and η in the cross-sectional plane are curvilinear–orthogonal, while the third coordinate ζ is rectilinear and aligned with the axes of the tubes. Associated with coordinates ξ and η are the spatially-varying metric coefficients h_ξ and h_η, which connect increments of ξ and η to increments of physical distance. The values of these metrics for any particular shape of cross-section are calculated by a numerical procedure described in ref. [11]. Since

the third coordinate ζ is rectilinear, the corresponding metric coefficient h_ζ is equal to unity.

For a steady three-dimensional viscous flow, the momentum conservation equations in terms of coordinates ξ–η–ζ can be written in the following common form

$$\frac{1}{h_\xi h_\eta}\frac{\partial}{\partial\xi}(\rho u h_\eta \Phi) + \frac{1}{h_\xi h_\eta}\frac{\partial}{\partial\eta}(\rho v h_\xi \Phi) + \frac{\partial}{\partial\zeta}(\rho w \Phi) - \frac{1}{h_\xi h_\eta}\frac{\partial}{\partial\xi}\left(\mu\frac{h_\eta}{h_\xi}\frac{\partial\Phi}{\partial\xi}\right) - \frac{1}{h_\xi h_\eta}\frac{\partial}{\partial\eta}\left(\mu\frac{h_\xi}{h_\eta}\frac{\partial\Phi}{\partial\eta}\right) - \frac{\partial}{\partial\zeta}\left(\mu\frac{\partial\Phi}{\partial\zeta}\right) - S_\Phi = 0 \quad (1)$$

where Φ is the dependent variable, which may stand for the velocity components u, v, w, in the ξ, η, ζ directions, respectively; ρ, μ are the fluid density and viscosity, respectively; and S_Φ is the source term of property Φ, containing the appropriate pressure gradient term as well as terms arising from coordinate curvature. The full expressions for S_Φ may be found in ref. [11].

The continuity equation closes the system of equations (1), i.e.

$$\frac{1}{h_\xi h_\eta}\frac{\partial}{\partial\xi}(\rho u h_\eta) + \frac{1}{h_\xi h_\eta}\frac{\partial}{\partial\eta}(\rho v h_\xi) + \frac{\partial}{\partial\zeta}(\rho w) = 0. \quad (2)$$

The boundaries of the solution domain (Fig. 1(b)) include tube walls, symmetry planes and inlet and outlet planes. On a tube wall the velocity components u, v, w are set to zero, while on a symmetry plane the velocity normal to this plane is zero as are the normal gradients of the remaining velocity components. The way of imposing boundary conditions at the inlet and outlet planes is described in Sections 4.2.1, 4.3.1 and 4.4.1 for the cases of purely axial, purely transverse and oblique flow, respectively.

3. METHOD OF SOLUTION

Solution of equations (1) and (2) is performed by finite-difference means according to the method described in ref. [12] with appropriate modifications required for incorporating the curvilinear–orthogonal coordinates. Therefore, only a very brief outline of the method will be given here.

An example of a three-dimensional grid employed for the finite-difference solution is shown in the isometric view of Fig. 1(b) and in the cross-sectional view of Fig. 1(c). Generation of the grid for any particular shape of cross-section is performed by a numerical procedure described in ref. [11]. The pressures p are stored at grid nodes formed by the intersection of the three families of grid lines while the velocity components u, v, w are taken to lie midway between the pressures which drive them. The finite-difference equations for the velocity components are derived by approximate integration of the differential momentum equations (1) and over six-sided control volumes (Fig. 1(c)) whose faces are formed by coordinate surfaces and whose centres are nodes at which the velocity components are stored. Such assumptions about the distribution of u, v and w between nodes are made in the process, that the resulting difference scheme is a hybrid of central/upwind differencing depending on the ratio of convective/diffusive flux coefficients [12]. The resulting finite-difference equations are typically of the form

$$a_P \Phi_P = \Sigma a_n \Phi_n + S_{\Phi,P} \quad (3)$$
$$n = E, W, N, S, D, U$$

where coefficients 'a' express the combined effects of convection and diffusion and $S_{\Phi,P}$ is the integrated source term. The summation is over the six neighbours E, W, N, S, D, U of the central node P of each control volume (Fig.1(c)). The continuity equation (2) is used in conjunction with the momentum equations to derive a pressure perturbation equation of the general form of equation (3), which tend to drive the velocities towards the satisfaction of continuity. The resulting system of equations is solved by an iterative alternating-direction-implicit algorithm.

4. FLOW CASES EXAMINED

4.1. *Introductory remarks*

The general equations (1) and (2) are simplified here to simulate purely axial ($\Theta = 0°$), purely transverse ($\Theta = 90°$) and oblique ($0° < \Theta < 90°$) fully-developed flow. The simplifications applied result in a considerable reduction in computer storage and time compared with the general three-dimensional problem. The fineness of the grids employed for the numerical solution of the governing equations in each case has been defined by performing grid dependence tests [11].

4.2. *Limiting case of purely axial, fully-developed flow*

4.2.1. *Equations and boundary conditions.* In this case, the transverse components of the velocity are zero ($u = v = 0$) and, owing to the condition of full development, all derivatives with respect to the axial coordinate ζ vanish with the exception of the pressure gradient term $\partial p/\partial\zeta$. Therefore, the general equations (1) and (2) are reduced to the momentum equation in the ζ-direction, i.e.

$$\frac{1}{h_\xi h_\eta}\frac{\partial}{\partial\xi}\left(\mu\frac{h_\eta}{h_\xi}\frac{\partial w}{\partial\xi}\right) + \frac{1}{h_\xi h_\eta}\frac{\partial}{\partial\eta}\left(\mu\frac{h_\xi}{h_\eta}\frac{\partial w}{\partial\eta}\right) - \frac{\partial p}{\partial\zeta} = 0. \quad (4)$$

Since the axial coordinate ζ, in the above equation, appears only in the pressure gradient term $\partial p/\partial\zeta$, the solution can be confined to a single cross-sectional plane ξ–η. The term $\partial p/\partial\zeta$ is either prescribed as an input or adjusted during the course of the calculation to give the desired axial mass flow rate.

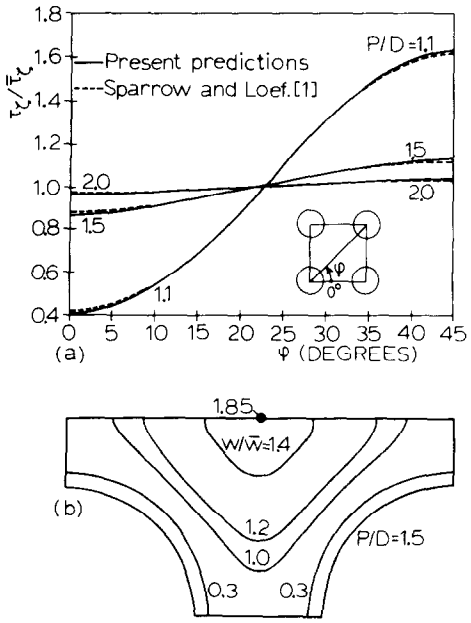

FIG. 2. Laminar, purely axial, fully-developed flow through square assemblies: (a) predicted variation of wall shear stress around the periphery of the tube; (b) predicted dimensionless velocity contours.

On the planes of symmetry LA, ABC, CH, IJ of the solution domain (Fig. 1(c)) the normal gradients of w-velocity are set to zero. On the tube surfaces LKJ and IH, $w = 0$.

4.2.2. *Results.* Calculations have been performed for square arrangements of various spacings. Comparisons of the results have been made with existing theoretical data, which showed that in the present limiting case of purely axial, fully-developed flow, the accuracy of the method is satisfactory: a maximum disagreement of less than 1.5% has been observed, which is within the limits of the truncation error of the numerical solution. Characteristic examples of the results are displayed in Fig. 2, discussed below.

Figure 2(a) shows the computed variation of the local wall shear stress τ_ζ (normalized by its average value $\bar{\tau}_\zeta$) around the periphery of the tube for square arrangements of pitch-to-diameter ratios $P/D = 1.1$, 1.5 and 2.0. The Sparrow and Loeffler [1] analytical solution, which appears in the same figure, is in very good agreement with the present results. Predicted dimensionless velocity contours $w/\bar{w}$ for the arrangement of $P/D = 1.5$ are shown in Fig. 2(b). Predicted values of the axial pressure drop coefficient c_{pa} for $P/D = 1.25$–2.00 are in very good agreement with the Sparrow and Loeffler [1] calculations, as shown in Fig. 5, which will be discussed later in Section 4.4.2.

4.3. *Limiting case of purely transverse, fully-developed flow*

4.3.1. *Equations and boundary conditions.* In this case, the general equations (1) and (2) are simplified by setting the axial velocity component w equal to zero and omitting all terms relating to the axial coordinate ζ. Therefore, the problem is described by the following equations.

Momentum equation in the ξ-direction

$$\frac{1}{h_\xi h_\eta}\frac{\partial}{\partial\xi}(\rho h_\eta u^2) + \frac{1}{h_\xi h_\eta}\frac{\partial}{\partial\eta}(\rho h_\xi uv) - \frac{1}{h_\xi h_\eta}\frac{\partial}{\partial\xi}\left(\mu\frac{h_\eta}{h_\xi}\frac{\partial u}{\partial\xi}\right) - \frac{1}{h_\xi h_\eta}\frac{\partial}{\partial\eta}\left(\mu\frac{h_\xi}{h_\eta}\frac{\partial u}{\partial\eta}\right) - S_u = 0. \tag{5}$$

Momentum equation in the η-direction

$$\frac{1}{h_\xi h_\eta}\frac{\partial}{\partial\xi}(\rho h_\eta uv) + \frac{1}{h_\xi h_\eta}\frac{\partial}{\partial\eta}(\rho h_\xi v^2) - \frac{1}{h_\xi h_\eta}\frac{\partial}{\partial\xi}\left(\mu\frac{h_\eta}{h_\xi}\frac{\partial v}{\partial\xi}\right) - \frac{1}{h_\xi h_\eta}\frac{\partial}{\partial\eta}\left(\mu\frac{h_\xi}{h_\eta}\frac{\partial v}{\partial\eta}\right) - S_v = 0. \tag{6}$$

Continuity equation

$$\frac{1}{h_\xi h_\eta}\frac{\partial}{\partial\xi}(\rho u h_\eta) + \frac{1}{h_\xi h_\eta}\frac{\partial}{\partial\eta}(\rho v h_\xi) = 0. \tag{7}$$

Solution of the above equations is confined to a single cross-sectional plane ξ–η because no variations exist in the axial direction ζ.

The assumption of full development implies that the flow repeats itself at the inflow and outflow boundaries AL and CH, respectively (Fig. 1(c)). This leads to the following practice for imposing the repeating boundary conditions at inflow and outflow boundaries: the grid is extended by one line FG, as shown in Fig. 1(c), and the velocity profile is transferred from line CH to line AL and from BK to FG after each iteration during the course of the calculation.

On the upper ABCF and the lower JI boundaries (Fig. 1(c)) of the solution domain, which are planes of symmetry, the normal velocity component v is zero as is the normal gradient of u-velocity. On the tube surfaces LKJ and IHG both velocity components are set to zero.

4.3.2. *Results.* Predictions have been obtained for in-line square arrangements of various spacings at transverse Reynolds number Re_t up to 500. Comparisons of the results with experimental data and numerical predictions from various sources showed that, in the present limiting case of purely transverse fully-developed flow, the accuracy of the method is satisfactory. Typical examples of the results are shown in Fig. 3 discussed below.

Figure 3(a) shows the predicted distribution of wall shear stress τ_ξ (normalized by the mean dynamic pressure $0.5\rho\bar{u}^2$) along the tube periphery for in-line square arrangements of $P/D = 1.25$ and 1.5 at a Reynolds number $Re_t = 10$. The calculations of Le Feuvre [7], which have also been plotted, are in very good agreement with the present predictions. The small negative shear stress regions, appearing in the

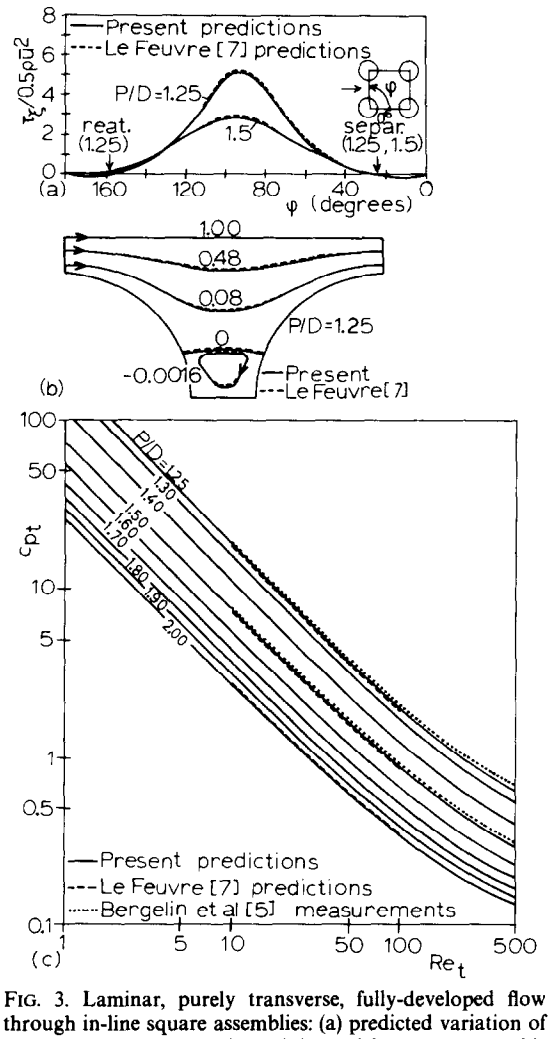

FIG. 3. Laminar, purely transverse, fully-developed flow through in-line square assemblies: (a) predicted variation of wall shear stress around the periphery of the tube at Reynolds number $Re_t = 10$; (b) predicted flow pattern at Reynolds number $Re_t = 10$; (c) transverse pressure drop coefficient vs Reynolds number for tube-to-diameter ratios $P/D = 1.25$–2.00.

same figure, correspond to the recirculation zone, which is clearly shown in the flow pattern plot of Fig. 3(b) for the arrangement of $P/D = 1.25$. The predicted streamline pattern of Le Feuvre [7], which is also plotted in this figure, is in very good agreement with the present predictions. It is noteworthy that in the closely spaced arrangement ($P/D = 1.25$) both separation and reattachment occur while in the widely spaced one ($P/D = 1.5$) only separation is observed, i.e. the recirculation zone does not bridge the whole gap between the tubes at $Re_t = 10$.

The predicted variation of the transverse pressure drop coefficient c_{pt} with Re_t for in-line square arrangements of $P/D = 1.25, 1.3, 1.4, \ldots, 1.9, 2.0$ is given in Fig. 3(c). The predictions of Le Feuvre [7] (available for $P/D = 1.25$, 1.50 and 2.00) and the experimental data of Bergelin *et al.* [5] (available for $P/D = 1.25$ and 1.50), which appear in the same figure, are in good agreement with the present predictions. For the higher Reynolds numbers, however, an increasing disagreement of both sets of predictions with the data is observed, which is due to the onset of the transition from laminar to turbulent flow.

4.4. *Fully-developed oblique flow*

4.4.1. *Equations and boundary conditions.* In this case, the flow is fully-developed in both the axial and the transverse directions and the bulk velocity makes an arbitrary, but uniform, angle with the tube axes. Under these circumstances there are no variations of flow conditions in the axial direction ζ, except from the pressure. Hence all derivatives with respect to ζ vanish, apart from the pressure gradient term $\partial p/\partial\zeta$. Therefore, the general equations (1) and (2) are simplified as follows: the momentum equations of the ξ- and η-directions and the continuity equation take the form of equations (5)–(7), respectively, while the momentum equation in the ζ-direction becomes

$$\frac{1}{h_\xi h_\eta}\frac{\partial}{\partial\xi}(\rho h_\eta u w) + \frac{1}{h_\xi h_\eta}\frac{\partial}{\partial\eta}(\rho h_\xi v w) - \frac{1}{h_\xi h_\eta}\frac{\partial}{\partial\xi}\left(\mu\frac{h_\eta}{h_\xi}\frac{\partial w}{\partial\xi}\right) - \frac{1}{h_\xi h_\eta}\frac{\partial}{\partial\eta}\left(\mu\frac{h_\xi}{h_\eta}\frac{\partial w}{\partial\eta}\right) + \frac{\partial p}{\partial\zeta} = 0. \tag{8}$$

An interesting feature of the governing equations (5)–(8) is that the transverse momentum equations (5) and (6) do not contain the axial velocity component w and are therefore decoupled from the axial flow, i.e. the latter has no influence on the transverse flow field. However, the converse is not true because the transverse velocity components u and v appear in the axial momentum equation (8). This absence of two-way coupling admits of the following particularly economical solution procedure: the transverse momentum equations (5) and (6) are solved together with continuity equation (7) by exactly the same procedure employed for the purely transverse flow of Section 4.3.1. The resulting u and v fields are then used as an input for solving the axial momentum equation (8). Solution of all equations is confined to a single cross-sectional plane ξ–η because the axial coordinate ζ appears only in the axial pressure gradient term $\partial p/\partial\zeta$. This term is either prescribed as an input or adjusted during the course of the solution to give the desired axial mass flow rate.

The usual boundary conditions are imposed on the tube surfaces and on the planes of symmetry, i.e. on the former, the velocity components are set to zero while on the latter, the normal velocity component is zero as are the normal gradients of the remaining components.

4.4.2. *Results.*

(a) *Velocity and wall shear stress distribution*

Figures 4(a) and (b) correspond to an in-line square arrangement of $P/D = 1.25$ and show the calculated axial and transverse flow fields in the form of dimensionless axial velocity contours $w/\bar{w}$ and streamline

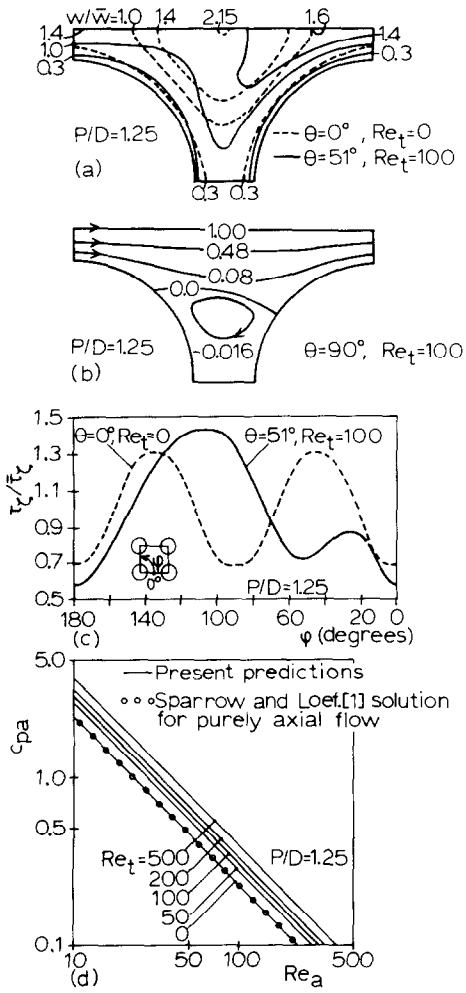

FIG. 4. Laminar, oblique, fully-developed flow through an in-line square assembly of pitch-to-diameter ratio $P/D = 1.25$: (a) predicted dimensionless axial velocity contours at $Re_t = 0$ (purely axial flow) and $Re_t = 100$; (b) predicted transverse flow field at $Re_t = 100$; (c) predicted variation of the axial wall shear stress around the periphery of the tube at $Re_t = 0$ (purely axial flow) and $Re_t = 100$; (d) predicted variation of axial pressure drop coefficient in terms of the axial Reynolds number for various values of the transverse Reynolds number.

pattern, respectively. The axial and transverse Reynolds numbers are $Re_a = 81$ and $Re_t = 100$, giving an inclination angle of the mean velocity vector to the tube axes $\Theta = \arctan(\bar{u}/\bar{w}) = \arctan(Re_t/Re_a) = 51°$. In the first of these figures, the predicted axial velocity contours for purely axial, fully-developed flow ($\Theta = 0°$, $Re_t = 0$) have also been plotted for comparison. It is observed that, as expected, these are symmetrical about the vertical bisector of the cross-section with the maximum dimensionless velocity $(w/\bar{w})_{max} = 2.15$ lying at the point furthest removed from the tube walls. The effect of transverse flow is to destroy the symmetry of the axial motion: the velocities near the downstream tube are increased while a decrease is observed behind the upstream tube, apart from the regions near the inlet and near the rearward stagnation point of this tube. The maximum dimensionless velocity $(w/\bar{w})_{max}$ is decreased from 2.15 to 1.6 and its location is 'convected' towards the outlet of the cross-section. These effects were due to the redistribution of the axial momentum provoked by the transverse flow. The latter tends to transfer high-momentum fluid from the centre towards the downstream tube and low momentum fluid from the boundary layer of the upstream tube into its wake. The increase of velocities near the rearward stagnation point of the upstream tube is due to the transport there of high momentum fluid by the recirculation zone. The latter is clearly shown in the transverse flow pattern of Fig. 4(b). With reference to this figure, it is recalled that although the axial velocity distribution is strongly influenced by the transverse motion, as described above, the latter is not influenced by the axial motion.

The calculated variation of the axial wall shear stress τ_ζ (normalized by the average axial wall shear stress $\bar{\tau}_\zeta$) around the periphery of the tube for the same tube arrangement and inclination angle as above, is shown in Fig. 4(c). In the same figure, the calculated distribution of $\tau_\zeta/\bar{\tau}_\zeta$ for purely axial, fully-developed flow is also plotted for comparison: it is clear that, in the oblique flow case, symmetry is destroyed thus showing the distorting influence of the transverse flow component. Higher shear stress values are now obtained at the front of the tube than at its rear and the two local maxima are displaced towards the rearward stagnation point of the tube.

(b) *Pressure drop coefficient*

It has been mentioned earlier that the transverse flow field is independent of the axial one. Therefore, the transverse pressure drop coefficient c_{pt} is a function of the transverse Reynolds number Re_t, not of the axial Reynolds number Re_a or the inclination angle Θ. The predicted effect of Re_t on c_{pt} has already been shown in Fig. 3(c).

The predicted variation of the axial pressure drop coefficient c_{pa} in terms of Re_a with Re_t as a parameter is displayed in Fig. 4(d), which corresponds to the same tube arrangement, discussed in the previous subsection. It is seen in this figure that for constant value of the transverse Reynolds number Re_t, the axial pressure drop coefficient c_{pa} varies inversely with the axial Reynolds number Re_a as in purely axial flow. The effect of transverse flow is to increase c_{pa} uniformly by an amount which is a function of Re_t. The minimum c_{pa} is observed at $Re_t = 0$, thus showing that the axial component of the flow is distributed in purely axial flow in such a way as to provide the least resistance. Noteworthy is the very good agreement of the predicted c_{pa} vs Re_a curve for purely axial flow ($Re_t = 0, \Theta = 0°$) with Sparrow and Loeffler's [1] analytical solution, which has been plotted in the same figure.

The nature of the variation of c_{pa} in terms of Re_a and Re_t discussed above, is also shown in the more

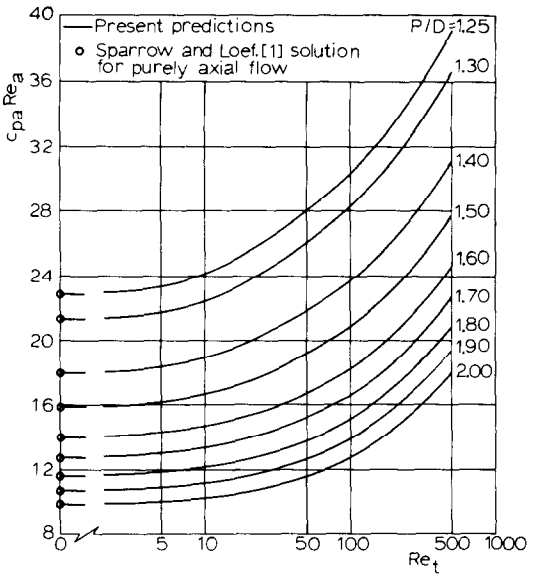

FIG. 5. Predicted variation of the product $c_{pa}\,Re_a$ in terms of the transverse Reynolds number for laminar, oblique, fully-developed flow through in-line square assemblies of pitch-to-diameter ratio P/D = 1.25–2.00.

compact representation of Fig. 5. Here, the predicted values of the product $c_{pa}\,Re_a$ have been plotted vs Re_t for in-line square arrangements of the whole range of pitch-to-diameter ratios examined, i.e. for P/D = 1.25–2.00. The values of $c_{pa}\,Re_a$ for purely axial, fully-developed flow, calculated by Sparrow and Loeffler [1], have also been plotted in Fig. 5. These are in very good agreement with the present predictions at $Re_t = 0 (\Theta = 0°)$ for all values of P/D. The same figure confirms that for increasing Re_t, i.e. for increasing inclination angle $\Theta = \arctan(Re_t/Re_a)$, the axial pressure drop coefficient c_{pa} increases considerably. This is due to increasing distortion of the axial velocity distribution, provoked by the transverse component of the oblique flow. The practical significance of these findings lie in the fact that it seems to be current practice to ignore the effect of inclination angle. For example, the ESDU [10] publication recommends that for Reynolds numbers Re (based on the mean velocity of the oblique flow) less than 50 and inclination angles Θ higher than 30°, the effect of Θ may be neglected, as will be discussed later.

Of great practical interest are the values of the pressure drop coefficient c_p in the direction of the mean velocity vector V of the oblique flow. The diagrams of Fig. 6 show the calculated c_p as a function of the Reynolds number Re (based on the magnitude of this vector), with the inclination angle Θ as a parameter. These results correspond to in-line square arrangements of P/D = 1.25, 1.3, 1.4,...,1.9, 2.0. The c_p vs Re curves for $\Theta = 90°$ are identical to the c_{pt} vs Re_t curves of Fig. 3(c), while for $\Theta = 0°$ they represent the purely axial flow relation $c_{pa}\,Re_a$ = const. of Fig. 5 at $Re_t = 0$. Therefore, the results of Fig. 6 are, in the limiting cases of $\Theta = 90°$ and 0°, in good agreement with Bergelin *et al.*'s [5] data and Sparrow and Loeffler's [1] calculations already shown in Figs. 3(c) and 5, respectively. However, for $0° < \Theta < 90°$ there is no information against which the present results may be tested, apart from the ESDU [10] correlation, mentioned earlier. According to this for $Re \leqslant 50$ and $\Theta > 30°$, the c_p vs Re relation is represented by a single curve, i.e. the one for purely transverse flow. The present calculations of Fig. 6 suggest that this is not the case. The reason for the disagreement is that the ESDU [10] correlation is based on the approximation that oblique flow past round tubes is equivalent to transverse flow past elliptical tubes, for which some information is available from Masliyah's [13] work. It is noteworthy that, as seen in Fig. 6, the c_p vs Re curves corresponding to $\Theta = 0°$ and 90° come closer to each other for increasing tube spacing and therefore the ESDU [10] correlation becomes more accurate.

5. CONCLUSION

The values of pressure drop in the case of laminar, oblique, fully-developed flow through in-line square tube assemblies of pitch-to-diameter ratio P/D = 1.25–2.00 and for inclination angles $0° \leqslant \Theta \leqslant 90°$ have been calculated in detail. Although this information is of great practical interest, it has not been available thus far. Unfortunately, support of these numerical predictions is not possible, owing to the seemingly total absence of detailed experimental data for this flow case. However, comparisons with theoretical and experimental data in the limiting cases of purely axial and purely transverse flow showed that the method of calculation is reliable at least in these limiting cases. The main conclusions may be summarized as follows.

The transverse flow field is independent of the axial one. Therefore, the transverse pressure drop coefficient c_{pt} is a function of the transverse Reynolds number Re_t and not of the axial Reynolds number Re_a or of the inclination angle Θ. The dependence of c_{pt} on Re_t is the same as in purely transverse fully-developed flow.

The axial pressure drop coefficient c_{pa} is related to the axial Re_a and the transverse Re_t Reynolds numbers as follows: for fixed values of Re_t, the $c_{pa}\,Re_a$ = const. relation of purely axial flow is retained. The value of the product $c_{pa}\,Re_a$ increases with Re_t. The minimum $c_{pa}\,Re_a$ is obtained in purely axial flow ($Re_t = 0$) where the axial velocity is distributed in such a way as to provide the least resistance. The rate of increase of $c_{pa}\,Re_a$ with Re_t diminishes with increasing tube spacing.

The pressure drop characteristics have been correlated on the basis of the pressure drop in the direction of the mean velocity vector and of the magnitude of this vector. The dimensionless parameters of the correlation are the oblique pressure drop coefficient

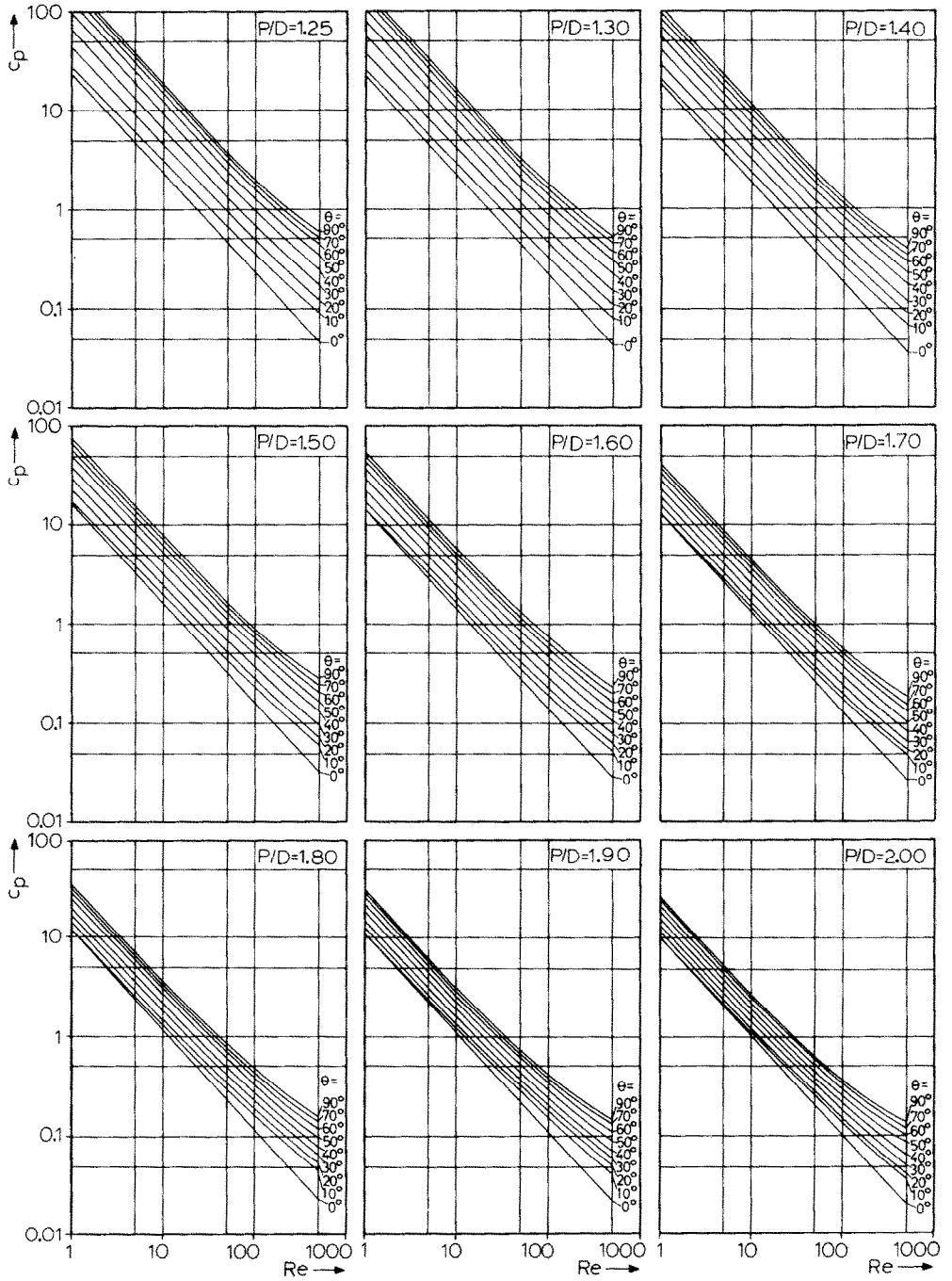

FIG. 6. Predicted pressure drop coefficient vs Reynolds number with the inclination angle Θ as a parameter for laminar, oblique, fully-developed flow through in-line square assemblies of pitch-to-diameter ratio $P/D = 1.25$–2.00.

c_p and the Reynolds number Re of the oblique flow. The calculated c_p vs Re curves suggest that the ESDU [10] recommendation to neglect the effects of inclination angle Θ, does not provide a good approximation. The influence of Θ on c_p becomes weaker for increasing tube spacing and the ESDU [10] approximation is then more realistic.

REFERENCES

1. E. M. Sparrow and A. L. Loeffler, Longitudinal laminar flow between cylinders arranged in regular array, *A.I.Ch.E. Jl* **5**, 325–330 (1959).
2. R. Meyder, Solving the conservation equations in fuel rod bundles exposed to parallel flow by means of curvilinear–orthogonal coordinates, *J. Comput. Phys.* **17**, 53–67 (1975).

3. K. Rehme, Pressure drop performance of rod bundles in hexagonal arrangements, *Int. J. Heat Mass Transfer* **15**, 2499–2517 (1972).
4. P. Carajelescov and N. E. Todreas, Experimental and analytical study of axial turbulent flows in an interior subchannel of a bare rod bundle, ASME Winter Annual Meeting, 75-WA/HT-51 (1975).
5. O. P. Bergelin, G. A. Brown and S. C. Doberstein, Heat transfer and fluid friction during flow across banks of tubes—part IV, *Trans. Am. Soc. mech. Engrs* **74**, 953–960 (1952).
6. A. Zhukauskas, Heat transfer from tubes in cross-flow, *Adv. Heat Transfer* **8**, 93–160 (1972).
7. R. F. Le Feuvre, Laminar and turbulent forced convection processes through in-line tube banks. Ph.D. thesis, Imperial College of Science and Technology, London (1973).
8. T. H. Massey, The prediction of flow and heat transfer in banks of tubes in cross-flow. Ph.D. thesis, Central Electricity Research Laboratories, Leatherhead, Surrey (1976).
9. W. M. Kays and A. L. London, *Compact Heat Exchangers*. McGraw-Hill, New York (1964).
10. ESDU, Pressure loss during cross-flow of fluids with heat transfer over plain tube banks without baffles, Engineering Sciences Data Item No. 74040 (1974).
11. K. A. Antonopoulos, Prediction of flow and heat transfer in rod bundles. Ph.D. thesis, Imperial College of Science and Technology, London (1979).
12. L. S. Caretto, A. D. Gosman, S. V. Patankar and D. B. Spalding, Two calculation procedures for steady, three dimensional flows with recirculation, *Proc. Third Int. Conference on Numerical Methods in Fluid Mechanics*, Vol. 2, pp. 60–68. Springer, Berlin (1972).
13. J. H. Masliyah, Viscous flow across banks of circular and elliptical cylinders: momentum and heat transfer, *Can. J. chem. Engng* **51**, 550–555 (1973).

PERTE DE CHARGE POUR UN ECOULEMENT LAMINAIRE, OBLIQUE, A TRAVERS DES ASSEMBLAGES DE TUBES EN LIGNE

Résumé—On calcule en détail des valeurs de la perte de charge subie par un écoulement laminaire, oblique et établi à travers des assemblages de tubes disposés en ligne avec des rapports pas/diamètre compris entre 1,25 et 2,00. L'angle d'inclinaison Θ du vecteur vitesse avec l'axe du tube varie dans le domaine $0° \leqslant \Theta \leqslant 90°$. Une nouvelle information est donnée sur l'influence de cet angle sur la perte de charge. La méthode de calcul est basée sur les différences finies appliquées aux équations de continuité et de quantité de mouvement exprimées en coordonnées curvilinéaires orthogonales. La méthode est validée en comparant les résultats avec les données théoriques et expérimentales existantes pour les cas limites de l'écoulement purement axial ($\Theta = 0°$) et purement frontal ($\Theta = 90°$); car il n'existe pas de donnée pour $0° < \Theta < 90°$.

DRUCKVERLUST BEI LAMINARER, SCHRÄG AUFTREFFENDER STRÖMUNG DURCH FLUCHTENDE ROHRANORDNUNGEN

Zusammenfassung—Es wird der Druckverlust berechnet, der bei laminarer, schräg auftreffender, voll entwickelter Strömung durch fluchtende quadratische Rohranordnungen auftritt, deren Teilungs-Durchmesser-Verhältnis im Bereich von 1,25 bis 2,00 liegt. Der Neigungswinkel Θ zwischen dem mittleren Geschwindigkeitsvektor und den Rohrachsen wird im Bereich von $0° \leqslant \Theta \leqslant 90°$ variiert. Neue Erkenntnisse über den Einfluß des Neigungswinkels auf den Druckverlust werden vorgestellt. Die Berechnungsmethode basiert auf einer Differenzenlösung der Impuls- und Kontinuitätsgleichung in gekrümmt-orthogonalen Koordinaten. Die Berechnungsmethode wird überprüft durch Vergleich der Ergebnisse mit vorhandenen theoretischen und experimentellen Befunden für die Grenzfälle einer rein axialen Strömung ($\Theta = 0$) und einer reinen Queranströmung ($\Theta = 90°$), da keine Ergebnisse für den Bereich $0° < \Theta < 90°$ vorliegen.

ПАДЕНИЕ ДАВЛЕНИЯ ПРИ ЛАМИНАРНОМ НАКЛОННОМ ТЕЧЕНИИ ЧЕРЕЗ КОРИДОРНЫЙ ПУЧОК ТРУБ

Аннотация—Дан детальный расчет падения давления при ламинарном наклонном полностью развитом течении через коридорный пучок труб квадратного сечения с отношением высоты к диаметру от 1,25 до 2,00. Угол наклона вектора средней скорости Θ к оси трубы изменялся в диапазоне $0° \leq \Theta \leq 90°$. Представлены новые данные по влиянию угла наклона на падение давления. Уравнения движения и неразрывности решаются методом конечных разностей в гауссовых координатах. Метод обоснован сравнением полученных результатов с существующими теоретическими и экспериментальными данными в предельных случаях чисто осевого ($\Theta = 0°$) и чисто поперечного ($\Theta = 90°$) потоков, поскольку таких данных для $0° < \Theta < 90°$ не имеется.